

THREE DIMENSIONAL BOUNDARY LAYER TRANSITION ANALYSIS IN SUPERSONIC FLOW USING A NAVIER-STOKES CODE

Yoshine Ueda, Hiroaki Ishikawa, Kenji Yoshida
Japan Aerospace Exploration Agency (JAXA), Tokyo, Japan

Keywords: *CFD, NS, 3-D boundary layer, T-S instability, cross-flow instability, sharp cone*

Abstract

The authors tried to improve the accuracy of transition analysis in supersonic flow by combining a usual e^N method and a Navier-Stokes computation. Transition characteristics of a sharp cone and a nose cone with non-zero angle of attack, and a supersonic natural laminar flow (NLF) wing designed by our agency were analyzed. The Navier-Stokes code was used for the estimation of the three-dimensional laminar boundary layer profiles that are the greatest controlling factor of the accuracy of the e^N method. Transition location on the side surface of the sharp cone and nose cone moved forward significantly in comparison with that on the top and the bottom lines of the bilateral symmetry plane. It is dominated by the crossflow instability on the whole surface except extremely near the top and the bottom lines. Strong forward movement of transition was only found on the top line of the sharp cone. It is based on the instability due to the inflection point of two-dimensional laminar boundary layer profile. It became clear that the transition location estimated by the present analysis was in the rear of the wing as compared to the result by the 3-dimensional boundary layer code with the conical flow approximation by Kaups-Cebeci. This was caused by over estimation of the crossflow near the leading edge of the wing under the influence of the approximation. Therefore, it is thought that the highly accurate laminar boundary layer has large influence on estimating critical Reynolds number.

Establishment of a transition prediction method is one of the important subjects in engineering. Today, the e^N method based on the stability theory of a laminar boundary layer is used as the most effective technique, and many analyses are tried at low speed and transonic speed [1]. However, a transition analysis at supersonic speed is limited to simple configurations like a sharp cone. It is originated in difficulty of obtaining effective transition data because usual supersonic wind tunnels have relatively large freestream turbulence. However, the sharp cone of 10° of apex is adopted as a standard model of transition study, and then the transition database by wind tunnel tests and flight tests is constructed [2].

However, even such a simple sharp cone, if it has non-zero angle of attack, a flow field becomes remarkably complicated. Thus, the transition characteristics become less simple. Although typical examples of experimental and numerical studies on the sharp cone at $M=3.5$ are demonstrated in reference [3] and [4], transition studies on axisymmetrical bodies with non-zero angle of attack in supersonic flow are not enough to understand its mechanism and to establish any transition prediction methods.

Japan Aerospace Exploration Agency (JAXA) has been promoting the scaled supersonic experimental airplane project as a part of developing the design technologies of a next generation SST. In this project, an original supersonic natural laminar flow wing design concept has been developed [5], and the actual validation of the effect is planned by flight tests with the airplane. A transition analysis tool was needed in the development process of the airplane. Although the program code [6] based

1 Introduction

on the e^N method was already spread widely in the USA, it was still difficult for us to obtain the code. Therefore, we have originally developed an analysis code [7], and then performed analysis and evaluation of the transition characteristics of the experimental airplane [8]. Qualitative validation of the effect of the supersonic natural laminar flow wing concept was also performed by wind tunnel tests [9].

In general, the accuracy of transition analysis based on the e^N method strongly depends on the accuracy of laminar boundary layer analysis. In the experimental airplane project, the Kaups & Cebeci method [10] was used for the analysis of laminar boundary layer. This method was also used in the above mentioned e^N code [6]. The method introduces the conical flow approximation to simplify the three-dimensional boundary layer equations. The approximation means no pressure gradient along the radial axis in the polar coordinate system shown in Fig. 1. It is mainly considered that the approximation is effective in the high aspect ratio wing. However, in the low aspect ratio wing with a highly swept leading edge and a warped surface like an SST, the approximation does not provide the sufficient accuracy of estimating the laminar boundary layer along the curved streamline near the leading edge.

To realize the high accurate analysis of a laminar boundary layer, we should solve the complete laminar boundary layer equation formulated in a general curvilinear coordinate system. However, the method of solution of such an equation system is very complicated. In general, CFD analysis is used abundantly for estimating the accurate pressure distribution on the whole surface of complicated configurations. Therefore, it is very effective and efficient that a Navier-Stokes analysis is directly applied to estimate a laminar boundary layer profile.

In this study, we constructed the transition analysis procedure which consisted of both a CFD code for laminar boundary layer profiles and our original e^N code for stability computation and integration of amplification rates of small disturbances. In the development of this procedure, we devised grid resolution, and we made an interpolation program for

estimating three-dimensional laminar boundary layer profiles and several physical quantities along outer streamlines over a configuration. By using this procedure, we were able to treat not only the highly accurate transition analysis about the natural laminar flow wing but also the transition characteristics of the above-mentioned axisymmetrical bodies with non-zero angle of attack.

First of all, the accuracy of the estimated result of the laminar boundary layer in the Navier-Stokes (NS) code was investigated through the analysis of the axisymmetrical bodies at 0° angle of attack. This was performed by comparing the NS-based laminar boundary layer profiles with the results of the already established axisymmetrical laminar boundary layer code [11]. Next, transition characteristics at 2° angles of attack were analyzed. In particular, about the transition analysis of the sharp cone, we took up the wind tunnel test in reference [12]. Then, we tried physical consideration to the feature of the transition characteristics in comparison with the analysis results.

Moreover, in case of the natural laminar flow wing, we compared the boundary layer profile by the Kaups & Cebeci method [10] with that by the NS code, and then considered the differences of N factor distributions based on those profiles. Here, the N factor is qualitatively corresponding to transition location. In addition, the validity of the conical flow approximation of Kaups & Cebeci code was also examined using whole pressure distributions on the surface at the design angle of attack (2°) by the NS code.

As above, the experimental transition data are required in establishing the practical transition prediction method based on the e^N method. Unfortunately, construction of such a transition database at supersonic speed is incomplete at present. Therefore, in this study, we pay attention only to the N factor distributions (or pattern) because the quantitative prediction of transition locations is not possible. For that reason, investigation of quantitative prediction is taken as the future subject.

The outline of our e^N method and CFD

(NS) analysis are summarized in section 2. The results of transition analysis on the sharp cone, the nose cone, and the natural laminar flow wing of the experimental airplane are described in section 3, 4 and 5 respectively.

2 Outline of Transition Analysis Procedure with CFD

2.1 Outline of e^N Method Based on Linear Stability Theory

In general, the next formalism is used in the spatial linear stability theory of a 3-dimensional laminar boundary layer. First, parallel flow approximation is applied to the laminar boundary layer, and then small disturbance of a following plane wave type is assumed.

$$q'(x, y, z, t) = \tilde{q}(y) \exp[i(\alpha x + \beta z - \omega t)] \quad (1)$$

where

$$\alpha = \alpha_r + i\alpha_i, \quad \beta = \beta_r + i\beta_i : \text{complex}$$

$$\omega \equiv 2\pi f : \text{real}$$

Here, q' represents velocity, temperature, and density, etc.; x is a local streamline direction at the edge of the boundary layer; y is a boundary layer thickness direction; z is a crossflow direction perpendicular to them; α_r and β_r are the wave number vectors of disturbance in x and z directions, respectively; α_i and β_i are amplification rate in x and z direction, respectively; and f is frequency of disturbance.

Next, linearization is carried out by considering q' is very small. Moreover, if the boundary condition is imposed that disturbance is 0 at the edge of the boundary layer and the wall, the simultaneous equation which forms an eigenvalue problem will be derived. Although this equation is solved under the specified Reynolds number and f at every x station, certain auxiliary equations are needed because the simultaneous equation includes four independent variables $\alpha_r, \alpha_i, \beta_r, \beta_i$. (The following assumption was used in our procedure.)

Furthermore, the e^N method is applied to predict the transition locations. If the amplitude of disturbance at a neutral stability point and in the amplification region in the downstream are set to A_0 and A respectively, then the location where the A increased e^N times of A_0 is judged to be an onset of transition. In this assumption, N factor is obtained by the following equation.

$$N \equiv \ln\left(\frac{A}{A_0}\right) = \int_C (-\alpha_i dx - \beta_i dz) \equiv \int_C d\sigma \quad (2)$$

Here, C indicates an integral path. In general, there are any arbitrary manners of selection of the path in case of a 3-dimensional flow. Although some trials (models) about the path and auxiliary equations are already proposed [1][13][14], they have no theoretical completeness. Therefore, we adopted the following assumption for the simplicity.

First, since a small disturbance is assumed, it is thought that the disturbance is basically carried along a local streamline. Therefore, we focus on the integral path limited in the local streamline direction ($dz = 0$), and then use the following equation. (Refer to Fig. 1)

$$d\sigma = -\alpha_i (\psi, \bar{\psi} : \text{Re}(x), f) dx \quad (3)$$

$$\text{where } \psi \equiv \tan^{-1}\left(\frac{\beta_r}{\alpha_r}\right), \quad \bar{\psi} \equiv \tan^{-1}\left(\frac{\beta_i}{\alpha_i}\right)$$

Here, ψ means a propagation direction of a wave number. (0° corresponds to a local streamline direction, and 90° corresponds to a crossflow direction.)

Next, the assumption of $\bar{\psi} = 0^\circ$ was used, because we found out that N factor might become large most, in case of $\bar{\psi} = 0^\circ$ in the investigation study of the influence of $\bar{\psi}$ on eigenvalue α_i [8]. Finally, in order to decide the relation between ψ and α_i , the following envelope method [1], which was widely used by many researchers, were applied. That is,

$$N(\text{Re}(x) : f) = \int_C \text{Max}_\psi [-\alpha_i(\psi : \text{Re}(x), f)] dx \quad (4)$$

where $C = \text{local outer streamline}$

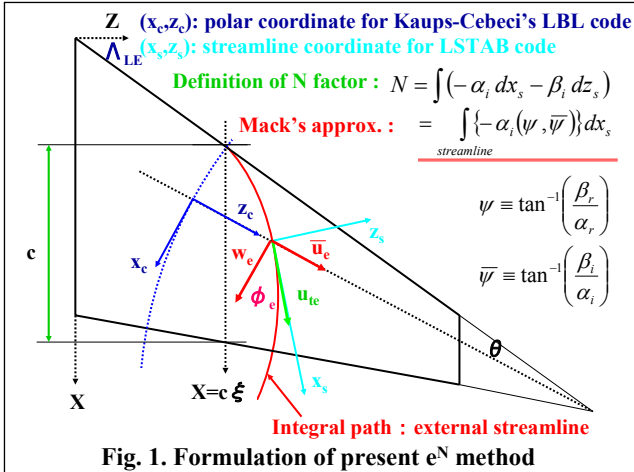
Here, $N(x)$ curves are evaluated for every f using above equation. Further, the following equation, which means the envelope of these N curves, is used as the final transition decision.

$$N_{\text{envelope}} = \text{Max}_f [N(\text{Re}(x) : f)] \quad (5)$$

(In addition, this analysis code is called “LSTAB” code for convenience in subsequent explanation.)

2.2 Outline of Laminar Boundary Layer Computation Code by Kaups & Cebeci

In nature of the eigenvalue equation, the first and the second derivatives of the profile in the thickness direction (y) are also needed. Thus, an analysis code of a 3-dimensional boundary layer which can estimate smooth profiles up to the second derivative is required. The method of reference [10] is relatively simple and is widely used because of conical flow approximation. The approximation means $\partial C_p / \partial z_c = 0$ (z_c indicates the radial coordinate shown in Fig. 1.) In this method, a boundary layer is computed along the arc x_c shown in Fig. 1. The estimated profile at each x_c station is transferred to the chordwise coordinates X at the spanwise station according to the conical flow approximation.



Moreover, if this coordinate system is used,

the integration of equation (4) has an advantage that numerical integration becomes easy because the equation becomes convertible into the integral of the chordwise coordinate dX by the analytical function based on the streamline direction and the planform geometry.

2.3 Outline of Transition Analysis Procedure with CFD

The transition analysis procedure consists of the following two steps. (A) First, the flow field and the laminar boundary layer on the surface of the object are estimated using the general-purpose CFD computation code called “UPACS” [15] of JAXA. (B) Next, the N factor that is concerned with a transition criterion is computed according to equation (5) using e^N method (LSTAB code). The subject on (A) and a comment of the integral path for the N factor are summarized below.

2.3.1 Outline of Grid Resolution of CFD Analysis

In order to estimate a laminar boundary layer profile required for a transition analysis, it was necessary to modify grid density so that many grid points would be concentrated in a boundary layer compared with the grid for the usual CFD analysis. Moreover, it was also necessary to modify the spacing in the direction of boundary layer thickness for decomposing a profile with high precision.

First, the laminar boundary layers on the sharp cone and the nose cone at zero angle of attack were analyzed using the CFD code at several kinds of resolution. Then, they were compared with the results estimated with the axisymmetrical boundary layer code [11]. Consequently, in case of the sharp cone as shown in Fig. 2, the minimum grid size in the direction of boundary layer thickness was set to $0.0135/(Re)^{0.5}$. In addition, it was found out that the grid resolution that was provided about 70 grid points in the boundary layer was effective. The total grid number was about five million points. Moreover, in case of the nose cone, the minimum grid size became effective at $0.058/(Re)^{0.5}$ by the same consideration, and the

total grid number became about four million points.

2.3.2 Selection Rule of Edge of Boundary Layer

In general, although the selection of the edge of a boundary layer is accompanied with some arbitrariness, the arbitrariness should not have any influence on boundary layer phenomenon essentially and physically. However, the LSTAB code has used boundary layer thickness as the reference length for making dimensionless for simplification of the formulation. Of course, the influence of boundary layer thickness is finally canceled out in the computation of N factor from the reason of the program structure.

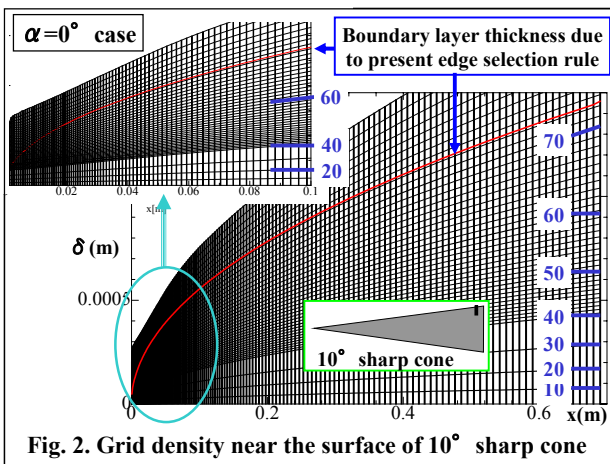


Fig. 2. Grid density near the surface of 10° sharp cone

However, it strongly requires the boundary layer thickness in the middle phase of computation. As a result, it has a weak point that a computation error remains. Moreover, in the LSTAB code, in order to integrate an amplification rate of a small disturbance wave in the direction of an external streamline on the edge of the boundary layer, highly accurate estimation of the direction and physical quantities (Mach number, temperature, etc.) becomes essential.

For the above reason, a modification of the system which estimates boundary layer thickness as sufficiently accurate as possible is needed in this transition analysis system. Thus, appropriate selection rule of the boundary layer edge were examined through comparing the NS-based boundary layer profiles with the profiles by the axisymmetric boundary layer code [11] about the sharp cone and the nose cone at 0°

angle of attack.

Consequently, by the selection rule for defining the point at 99.9% of the maximum velocity in the boundary layer as the boundary layer thickness, it became clear that a large error arose near the leading edge as shown in Fig. 3. It depends on that the boundary layer near the leading edge is extremely thin. Hence, it is thought the error accompanying interpolation at the point of 99.9% is amplified. Therefore, by paying attention to a derivative $d(\rho u)/dy$, we defined the point below a certain value (%) to the maximum value of the derivative in the boundary layer as the edge of the boundary layer. Of course, the value should be 0 strictly, but it is impossible to set 0 values in the continuous linking with the flow field of the outside of the boundary layer.

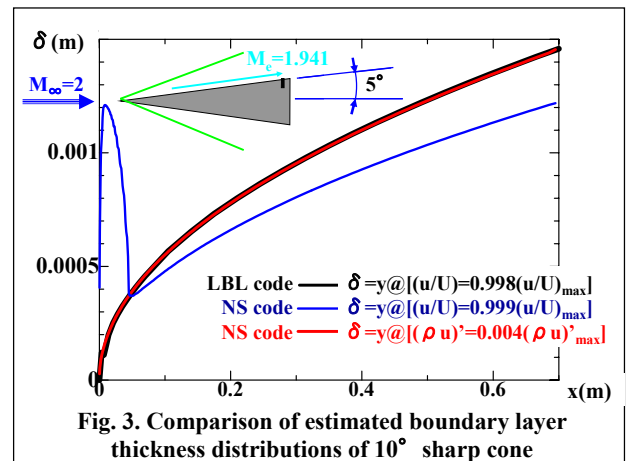


Fig. 3. Comparison of estimated boundary layer thickness distributions of 10° sharp cone

As a consequence of investigation, as shown in Fig. 3, when the value was set to 0.4% on the sharp cone, it became clear that it was almost completely in agreement with the result by the boundary layer code. Moreover, the result using the value 0.4% was good on the nose cone, but the degree of coincidence has been improved further when the value was set to 1.0%. If the solution by the boundary layer code was known in advance like this time, the above-mentioned values (0.4%: sharp cone, 1.0%: nose cone) were used then, and also in case of non-zero angle of attack, this selection rule was also applied directly.

2.3.3 Comment on Integral Path for Computation of N factors

Since the edge of the boundary layer is estimated in Navier-Stokes calculation as mentioned above, the direction of the local streamline can be estimated automatically. Therefore, it is considered that the integration of eigenvalue α_i is easily computable by the numerical integration. In this case, above-mentioned assistance of the analytical formulation becomes unnecessary.

3 Transition Analysis on 10° Sharp Cone

3.1 Case on 0° of Angle of Attack

As an analysis condition for the sharp cone, we took up the case of freestream Mach number 2.0 and unit Reynolds number 9 million because there was a database of a lot of wind tunnel and flight tests. In general, if a sharp cone has 0° angle of attack at supersonic speed, the boundary layer has self-similar feature because of lack of the representative length characterizing a flow direction. This means that dimensionless form of velocity and temperature profiles based on a displacement thickness are similar.

Therefore, first of all, checking the self-similar feature of the boundary layer profile was attempted as a part of validation of present procedure with the Navier-Stokes code. Fig. 4 shows the comparison of the velocity and the temperature boundary layer profiles at the three

different streamwise stations. From the fact that both profiles are overlapped completely at each station as shown in Fig. 4, the self-similarity is confirmed clearly. Thus, the accuracy of estimating the boundary layer by the NS code is considered to be sufficient.

Figs. 5 show the results of the stability analysis using the boundary layer profile of NS computation. In Fig. 5a, the propagation direction of the small disturbance wave with the maximum amplification rate using the CFD-based boundary layer profiles (solid line) is compared with the result using the axisymmetric boundary layer code [11] (broken line). The figure shows they coincide very well. Moreover, Fig. 5b shows N curves for each frequency by equation (4), and differences are very small even there are slight discrepancies between them. Thus, the results of the transition analysis with CFD (NS) code are considered to be appropriate sufficiently. In addition, the N factor distribution on the surface of the sharp

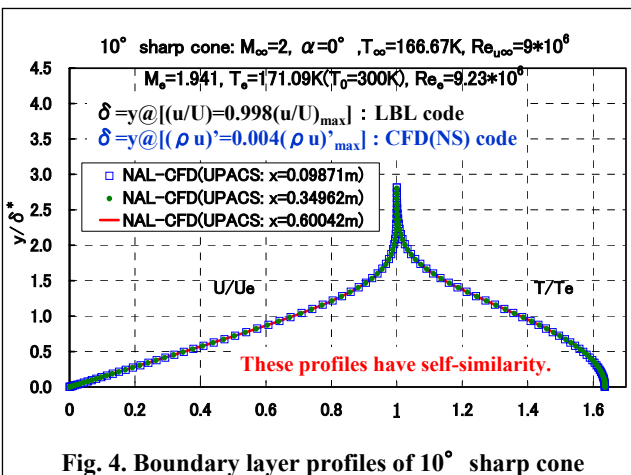


Fig. 4. Boundary layer profiles of 10° sharp cone

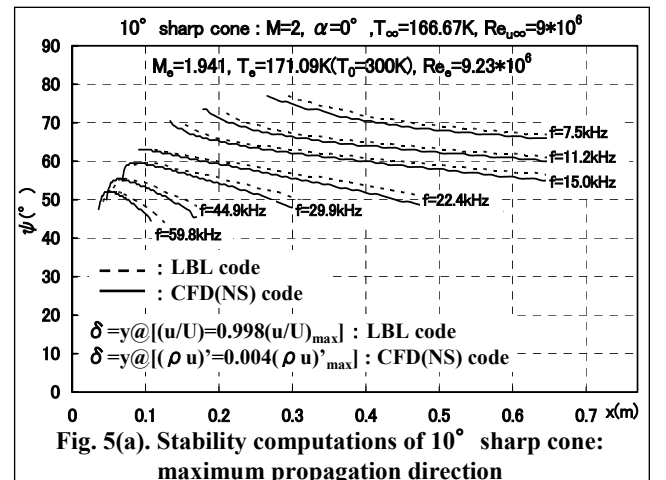


Fig. 5(a). Stability computations of 10° sharp cone: maximum propagation direction

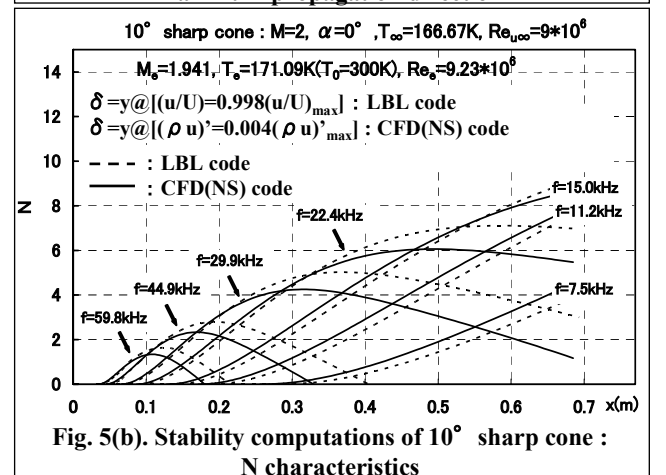


Fig. 5(b). Stability computations of 10° sharp cone : N characteristics

cone is also shown in Fig. 11 with broken lines, as demonstrated below.

3.2 Case on 2° of Angle of Attack

As a typical example of the case of non-zero angle of attack, the angle of 2° was selected here. The estimated external streamline by CFD analysis with the above-mentioned edge selection rule is shown in Fig. 6. A few representative streamlines are also shown in Fig. 7a. Here, for our convenience, we set the top line to #6, the bottom line to #96, and two streamlines on the side surface to #86 and #91 as naming of streamlines.

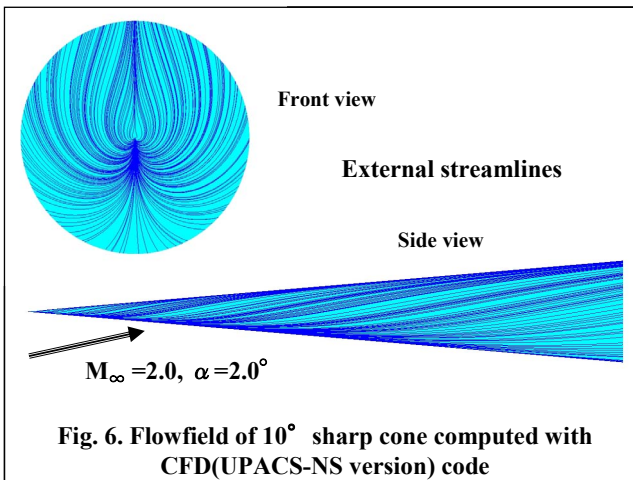


Fig. 6. Flowfield of 10° sharp cone computed with CFD(UPACS-NS version) code

First of all, it is seen in Fig. 7a that the Cp distribution on the top and bottom lines are almost constant in the flow direction. Moreover, they mutually shift same amount to the opposite direction against the result of 0° angle of attack. The flow on the top and bottom lines is two-dimensional and has no crossflow in the boundary layer.

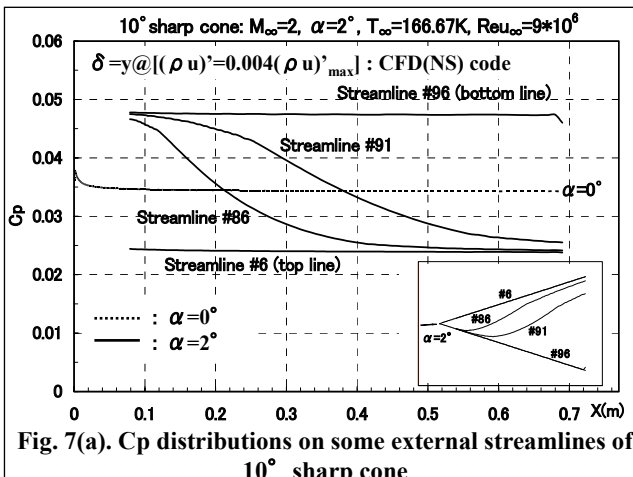


Fig. 7(a). Cp distributions on some external streamlines of 10° sharp cone

Boundary layer thickness distribution is shown in Fig. 7b. The thickness on the top line is relatively thicker than the thickness on the bottom line and the side lines. It is found that there is no factor that grows the boundary layer greatly because of no pressure gradient in the flow direction.

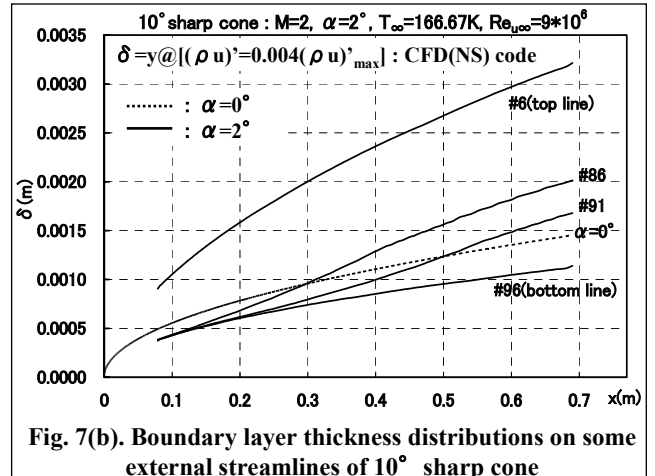


Fig. 7(b). Boundary layer thickness distributions on some external streamlines of 10° sharp cone

Fig. 8 shows the boundary layer profiles on the external streamline direction (U/U_e) and the crossflow direction (V/U_e) at a representative axial station ($x=0.6m$). Except the top and bottom lines, it is confirmed that the crossflow component has certainly induced. Moreover, on the top line, it turns out that the U/U_e profile is similar to the profile with an inflection point near separation. This is the true nature of the increase in the boundary layer thickness as shown in Fig. 7b. As there is no pressure gradient, we suppose that it is owing to 3-dimensional effect by flowing into the top line.

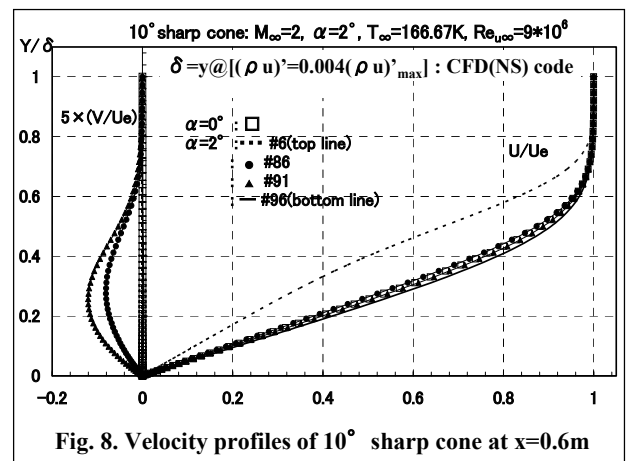


Fig. 8. Velocity profiles of 10° sharp cone at $x=0.6m$

In order to study this phenomenon, in the

face perpendicular to the axial direction in relatively rear of the sharp cone, the velocity profile near the top line and Mach number contour are shown in Fig. 9. In addition, the result on the below-mentioned nose cone is also shown in this figure for comparison. As we can guess mostly from Mach number contour, the boundary layer thickness is increasing near the top line on the sharp cone. On the other hand, such tendency is not seen on the nose cone.

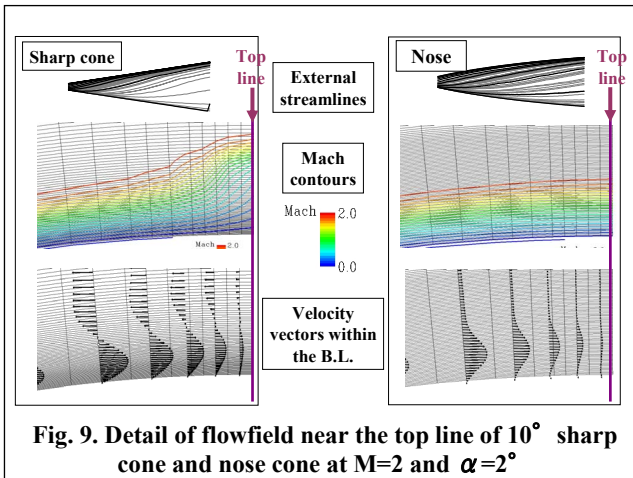


Fig. 9. Detail of flowfield near the top line of 10° sharp cone and nose cone at M=2 and $\alpha=2^\circ$

The velocity vectors on the sharp cone in the circumference direction indicate the inflow with relatively low speed fluid to the symmetric plane near the wall, and the outflow with relatively high speed fluid from the plane near the edge of the boundary layer. Therefore, the external streamlines slightly expand toward the circumference direction and downstream. This means the direction of the boundary layer thickness is a getaway of the flow that is flowed in from both sides toward the symmetric plane. Such flow feature is balanced by the rotational flow field.

On the other hand, the outflow from the symmetric plane is hardly seen on the nose cone. This probably depends on the fact that the low-speed fluid that flows into the symmetric plane near the wall is accelerated because of strong acceleration due to favorable pressure gradient in the axial direction. As a result, no flow in the direction of the boundary layer thickness is induced, and the inflow fluid is taken in through a deformation of the velocity profile in the symmetric plane. This expresses that the remarkable outflow from the symmetric plane is

not observed. Therefore, it is considered that the boundary layer thickness is not increased on the top line of the nose cone.

Furthermore, through investigating the pressure distribution in the boundary layer near the top line in detail, a remarkable pressure gradient was observed in case of the sharp cone. In general, boundary layer approximation does not contradict that a pressure gradient exists in a boundary layer which progresses on a surface having curvature. On the other hand, the large curvature of the external streamline on the nose cone is suppressed by the acceleration due to a favorable pressure gradient in the axial direction. Consequently, it is understood that the pressure gradient in the boundary layer is kept relatively uniform.

Next, Fig. 10a indicates the result of 2° (solid line) and 0° (O mark) angles of attack for the propagation direction with maximum amplification rate on the streamline #86. From

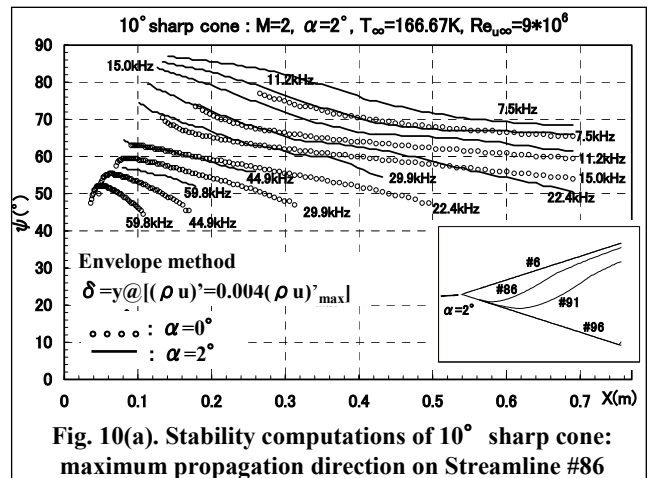


Fig. 10(a). Stability computations of 10° sharp cone: maximum propagation direction on Streamline #86

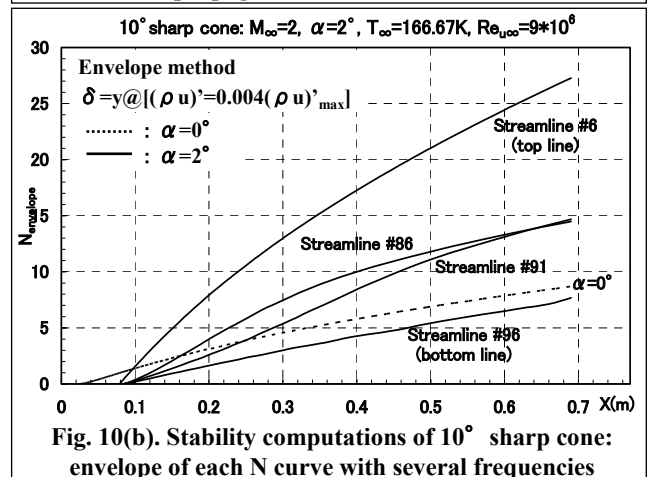


Fig. 10(b). Stability computations of 10° sharp cone: envelope of each N curve with several frequencies

the figure, it is seen that the direction increases to 80° - 90° on the side when it has a non-zero angle of attack. It is easily understood that crossflow instability is dominated in the case of non-zero angle of attack.

Fig. 10b shows the envelope of the N curves for each frequency estimated by equation (5). The figure shows that the N factor on the top line is very large. This tendency contradicts expectation that the N curves in Tollmien-Schlichting instability are smaller than that in crossflow instability. It cannot be overemphasized that this originates in the velocity profile on the above-mentioned top line. On the other hand, on the bottom line, it also turns out that it is decreasing in case of 0° angle of attack as we expected.

Fig. 11 shows a side view of the N factor distributions finally obtained. As an effect of angle of attack, it can be seen that the estimated transition location corresponding to a certain N factor, except on the bottom line, moves forward considerably. This tendency is qualitatively almost similar to the result of the transition measurement by King [3] as shown in the figure, in spite of different Mach number and angle of attack conditions. Thus, it is supported that this analysis result is appropriate. Moreover, it is also suggested in the reference [4] that transition on the top line is dominated by inflection point instability on two-dimensional boundary near separation. However, the transition location pattern near the top line is not clearly found out in reference [4].

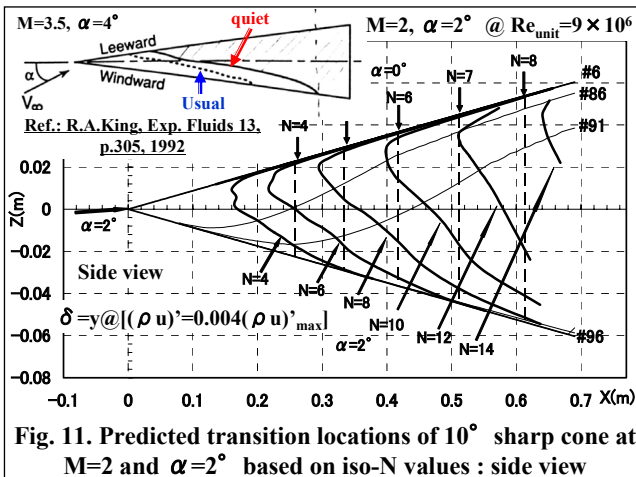


Fig. 11. Predicted transition locations of 10° sharp cone at $M=2$ and $\alpha=2^\circ$ based on iso-N values : side view

In order to investigate the transition location pattern on the sharp cone with non-zero angle of attack, transition measurement tests were carried out [12] as a part of fundamental technology research activities of our project. The wind tunnel of Fuji Heavy Industries (FHI) in Japan was used for the test because it had relatively low freestream turbulence due to in-draft driven system. Transition characteristic analysis at the test condition was also performed using this technique.

Figs. 12 show the comparison of the N factor distribution in the analysis and the transition location pattern measured with the infrared camera technique. Fig. 12a is a side view. If $N=6$ is assumed, the N factor distribution is qualitatively similar to the measured transition location.

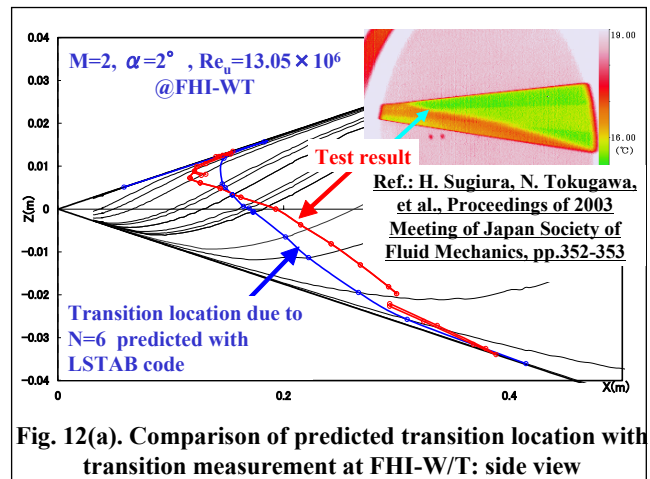


Fig. 12(a). Comparison of predicted transition location with transition measurement at FHI-W/T: side view

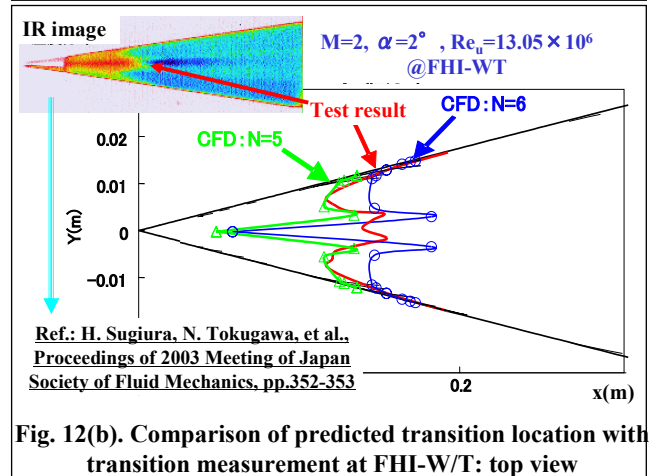


Fig. 12(b). Comparison of predicted transition location with transition measurement at FHI-W/T: top view

Fig. 12b is a top view. Here, it is seen that the result with $N=5$ is closer to the test result. Further, it was confirmed that the measured transition location on the top line also moved

forward a little as similar to the predicted one. Moreover, it is supposed that the possibility of promoting transition due to the separation type instability is supported.

However, the amount of the forward movement of transition location was quite deviated quantitatively. Naturally, the criterion of $N=6$ or 5 includes the influence of freestream turbulence in the tunnel. Therefore, we can not conclude that the principal mechanism for the forward movement of the transition on the top line is a cause based on our numerical consideration, as mentioned above, because of no experimental information [12] of boundary layer profile on the top line. It is necessary to advance further experiments for the transition behavior near the top line.

Finally, in order to understand quantitatively that crossflow was dominated on the side face of the sharp cone with non-zero angle of attack, we tried to simulate pseudo N factor distribution without crossflow instability

using the LSTAB code at no crossflow condition. The result is shown in Figs. 13. The broken lines in the figures are the result without the crossflow component. If there is no transition due to the crossflow instability (if only oblique T-S wave instability is a main factor), it turns out that all the transition locations move rearward except the top line.

This behavior may be easily understood from the favorable pressure gradient shown in Fig. 7, except for the top and bottom lines. Since it becomes an accelerated type toward downstream, it always leads to delaying amplification of the oblique T-S wave instability. However, because of any pressure gradient between such curved external streamlines, crossflow is always generated and the transition is brought forward according to the inflection point type instability. In the case of the sharp cone with non-zero angle of attack, it is found in Fig. 13b that the crossflow instability is dominated in all the regions excluding within about 10° from the top line.

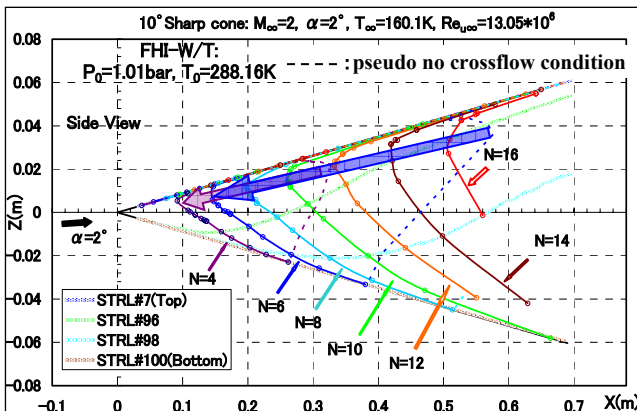


Fig. 13(a). Effect of crossflow instability based on pseudo no crossflow condition : side view

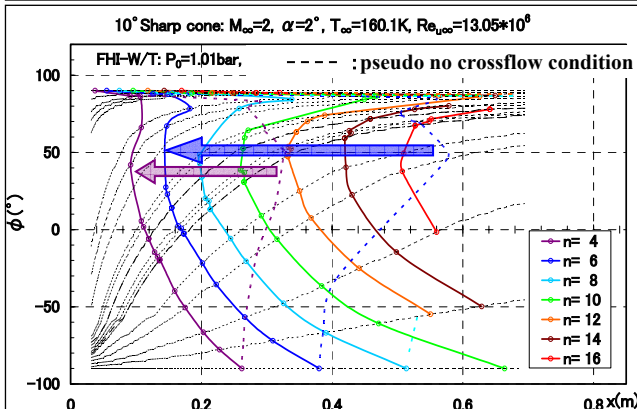


Fig. 13(b). Effect of crossflow instability based on pseudo no crossflow condition : circumference view

4 Transition Analysis on the Nose Cone of the Scaled Supersonic Experimental Airplane

The nose cone of the scaled supersonic experimental airplane (called “NEXST-1”) is the same as the front part of the Sears-Haack body by applying the area-ruled fuselage design method [5]. In the transition analysis on the nose cone, the same condition as the wind tunnel test in reference [12] was selected. It is planned to compare the analysis result with a transition measurement result which will be tried in the near future. The result of the transition analysis in the case of 2° angles of attack is described below.

First of all, using the above-mentioned selection rule of the edge of a boundary layer, the direction of an external streamline is estimated based on the velocity vector of the streamline. The pressure distributions on the typical streamlines are shown in Fig. 14a. Here, we named the top line as #1, the bottom line as #111, and two representative streamlines of the side as #90 and #102 in the figure. (Those

streamlines are indicated in Fig. 16.)

In the pressure distribution shown in Fig. 14a, the favorable pressure gradient on the top line is more moderate than that at the case of 0° angle of attack. The pressure gradient on the bottom line is increasing a little after the middle of nose length. Moreover, while the favorable pressure gradient near the apex of the nose cone is decreasing on the side surface of the cone, the pressure gradient is increasing toward rearward.

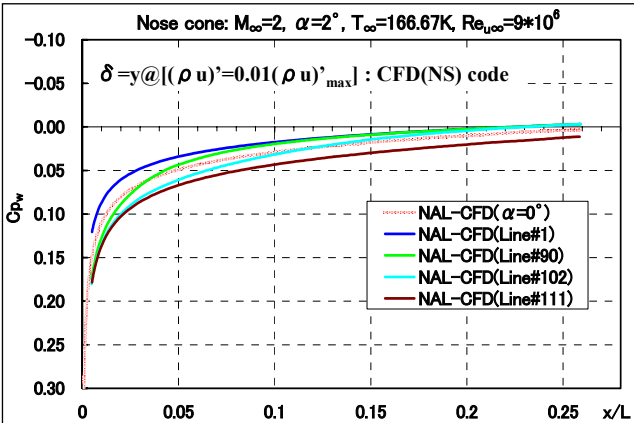


Fig. 14(a). Cp distributions on some external streamlines of NEXST-1 nose cone

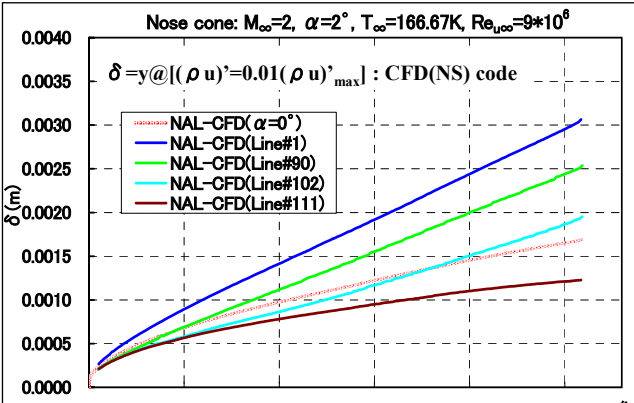


Fig. 14(b). Boundary layer thickness distributions on some external streamlines of NEXST-1 nose cone

According to these pressure distributions, we can easily understand the tendency of the boundary layer thickness distribution shown in Fig. 14b. The boundary layer thickness on the top line is large compared with the thickness on the bottom line and the side lines. This feature is the same as that of the sharp cone. However, through examining the velocity profile on the top line in detail (mentioned later), the increase of the thickness was confirmed to be unrelated to the profile near separation. Thus, it is concluded that the increase of the thickness

simply originates in the difference of the pressure gradient in the flow direction.

Fig. 15 shows the envelope of the N curves corresponding to each frequency. It is seen that the N factors of the envelope curves on the side surface are very large. Furthermore, the propagation direction with maximum amplification rate of a small disturbance wave was confirmed to be almost 80° - 90° . These results lead to the fact that crossflow instability is certainly dominated on the side surface. Here, although the envelope on the top line shown in Fig. 15 is decreasing in $0.22 < x/L$, it probably depends on some fluctuation in the physical quantity by CFD computation. Therefore, it is considered that this decrease is not essential tendency as the transition characteristics. Moreover, in case of the nose cone, as mentioned above, remarkable behavior on the top line of the nose cone is not seen as shown in the result of the sharp cone.

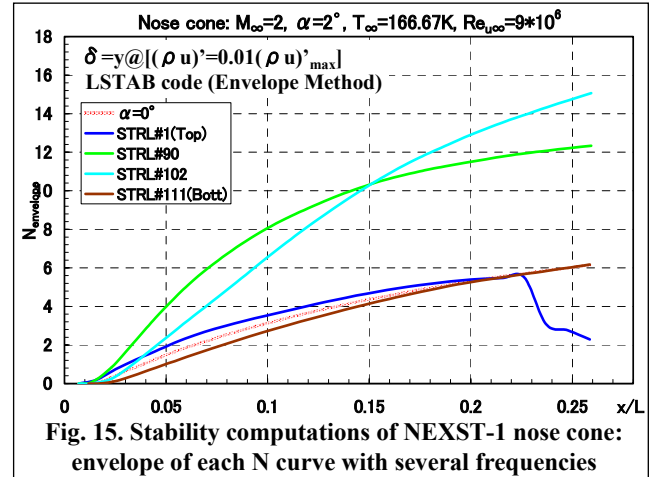


Fig. 15. Stability computations of NEXST-1 nose cone: envelope of each N curve with several frequencies

Figs. 16 show the N factor distribution obtained finally. It is seen that the estimated transition locations corresponding to each N factor are in rearward on the top and bottom lines, and are moving forward rapidly on the side surface. This means that the transition is controlled by the crossflow instability almost in the whole region, except the top and bottom lines. Further, the broken lines in the figure express the estimated result in case of 0° angle of attack.

Moreover, the comparison of the N factor distribution in top view of the sharp cone and the nose cone is shown in Fig. 17. (Here, this

analysis was performed at the same unit Reynolds number condition of 9 million. Therefore, it strictly differs from the result in Fig. 16. However, it is confirmed that the qualitative tendency is completely equivalent.)

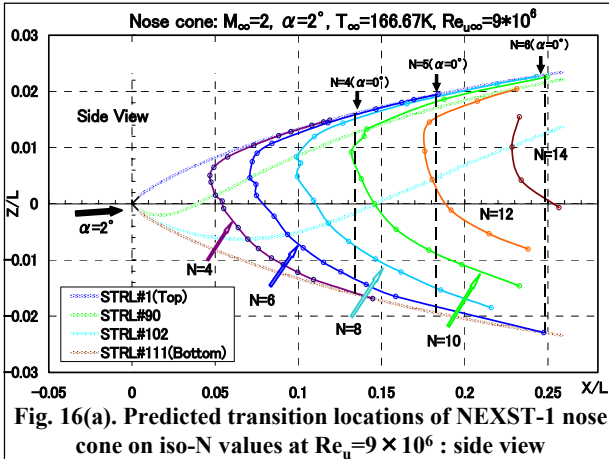


Fig. 16(a). Predicted transition locations of NEXST-1 nose cone on iso-N values at $Re_u=9 \times 10^6$: side view

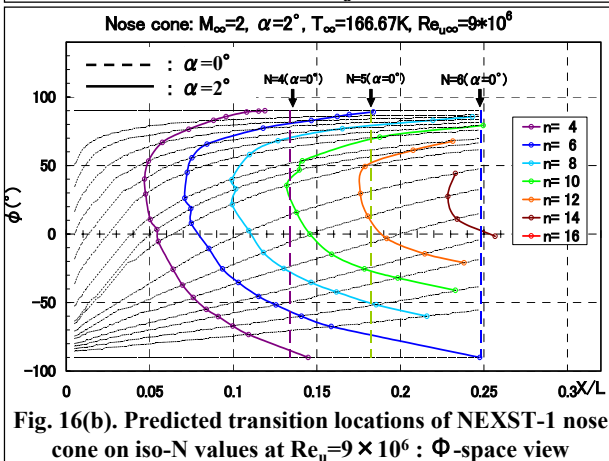


Fig. 16(b). Predicted transition locations of NEXST-1 nose cone on iso-N values at $Re_u=9 \times 10^6$: Φ -space view

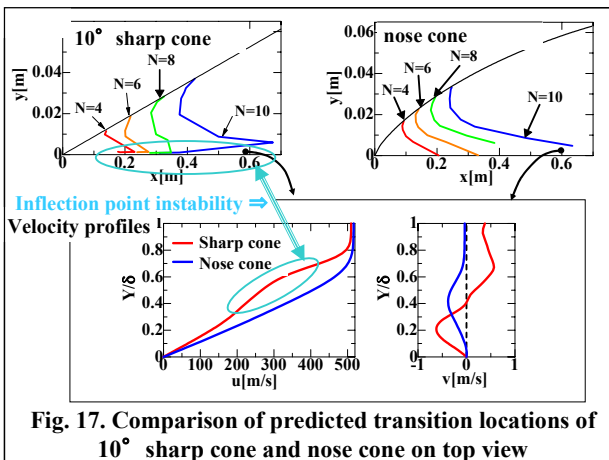


Fig. 17. Comparison of predicted transition locations of 10° sharp cone and nose cone on top view

It is seen in Fig. 17 that the region of the forward movement of transition location on the side surface is large on the nose cone. This is

interpreted that existence of the favorable pressure gradient on the nose cone tends to induce crossflow in a boundary layer. Moreover, the N factor distribution near the top line is completely different from the case of the sharp cone. This difference is easily understood from the remarkably different velocity profiles as shown in the figure. In particular, it is clear that the velocity profile on the nose cone is not the profile near separation.

5 Transition Analysis on the Natural Laminar Flow Wing of the Scaled Supersonic Experimental Airplane

The designed wing has the large curvature near the leading edge because of realization of the natural laminar flow at supersonic speed. In order to improve the estimation accuracy of the laminar boundary layer near the leading edge, the above-mentioned CFD analysis procedure was applied.

First of all, Fig. 18 shows CFD analysis result of the flowfield around the wing and fuselage at the design point of the experimental airplane (Mach number 2.0, angles of attack 2° , flight altitude 15km). A lot of thin lines in the figure are local streamlines of the edge of the boundary layer.

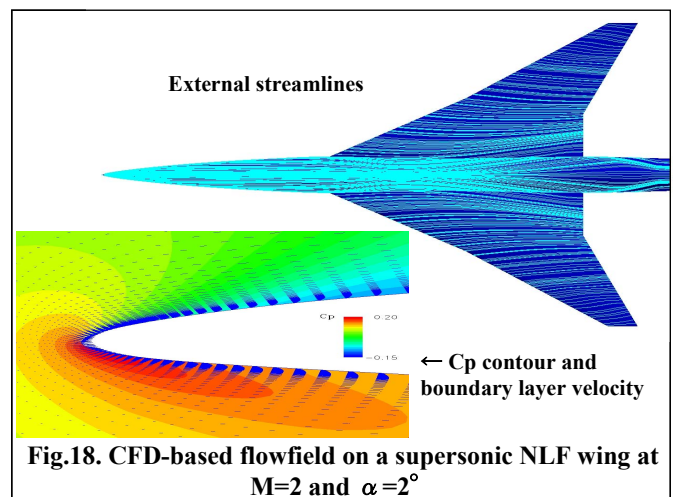


Fig.18. CFD-based flowfield on a supersonic NLF wing at $M=2$ and $\alpha=2^\circ$

Next, the validity of the conical flow approximation used in the Kaups & Cebeci method [10] was examined, based on the CFD-based pressure distribution on the wing surface.

**THREE DIMENSIONAL BOUNDARY LAYER TRANSITION
ANALYSIS IN SUPERSONIC FLOW USING A NAVIER-STOKES CODE**

Fig. 19a is a comparison of the chordwise pressure distribution at 30% semi-spanwise station. On the other hand, Fig. 19b shows the result of derivatives in the radial axis (z_c) direction of Fig. 1. (Here we used r as z_c for simplicity of notation.)

These figures show that conical flow approximation is not strictly realized on all locations in the chordwise direction at the 30% semi-spanwise station. Since these derivatives have dimension, they are made dimensionless by the local chord length as shown in the figure. Then, it can be compared with the pressure gradient of the averaged chordwise direction at $x/c=0.1-0.7$ in Fig. 19a. As a result, it became clear that about 5 times stronger pressure gradient exists in the radial axis direction. Therefore, it is supposed that the laminar boundary layer computation code of Kaups & Cebeci has a remarkable error in application on a low aspect ratio wing with a highly swept back angle like the experimental airplane.

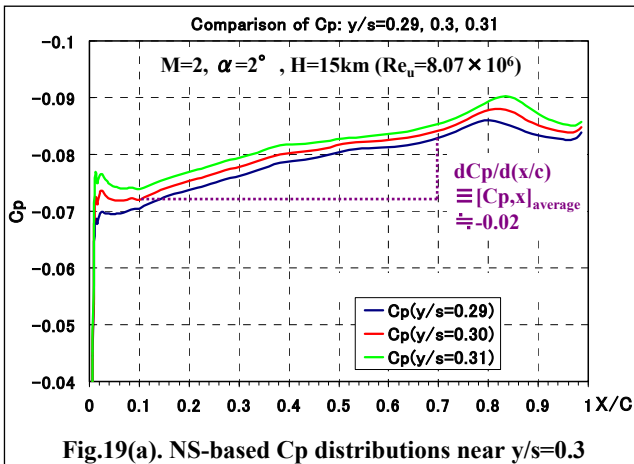


Fig.19(a). NS-based C_p distributions near $y/s=0.3$

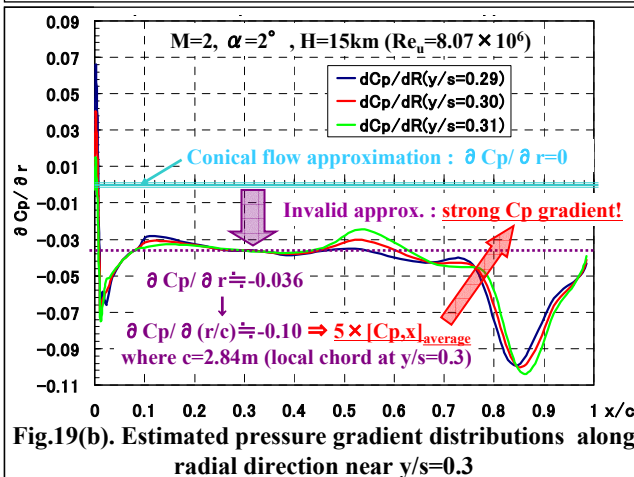


Fig.19(b). Estimated pressure gradient distributions along radial direction near $y/s=0.3$

The laminar boundary layer analyzed using the CFD code at the inboard wing (at $y/s=0.3$) and the outboard wing (at $y/s=0.7$) are summarized in Fig. 20. In this analysis, we were fortunately able to use a conventional simple edge selection rule that boundary layer thickness was treated as the position where velocity had 99.9% of the maximum velocity within the boundary layer. As shown in the figure, the CFD-based boundary layer thickness agrees mostly with the result by the boundary layer code [10] from the leading edge to the middle of the chord length.

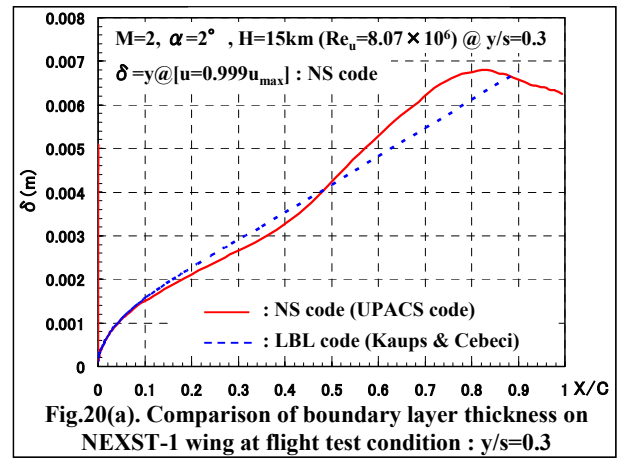


Fig.20(a). Comparison of boundary layer thickness on NEXST-1 wing at flight test condition : $y/s=0.3$

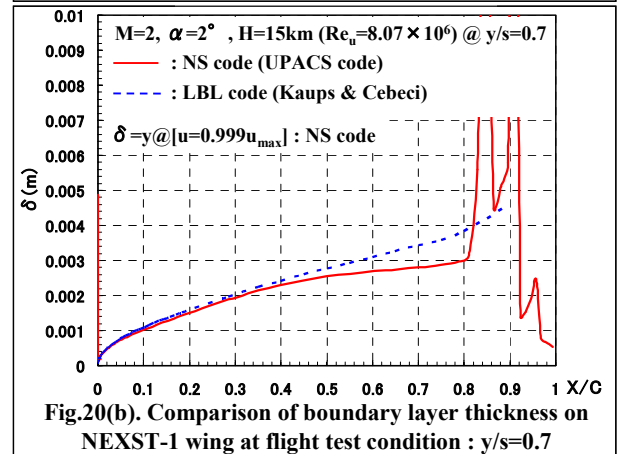


Fig.20(b). Comparison of boundary layer thickness on NEXST-1 wing at flight test condition : $y/s=0.7$

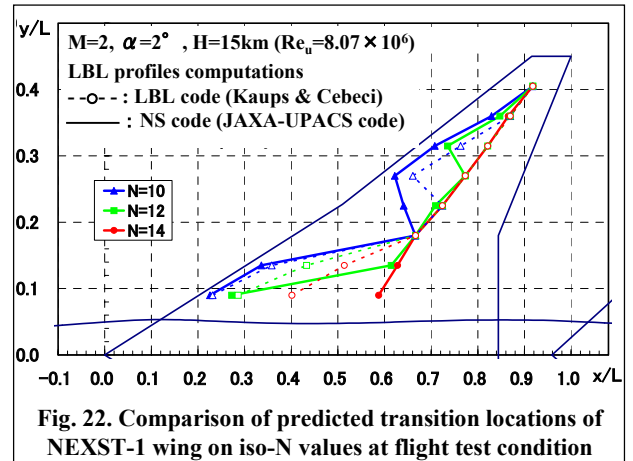
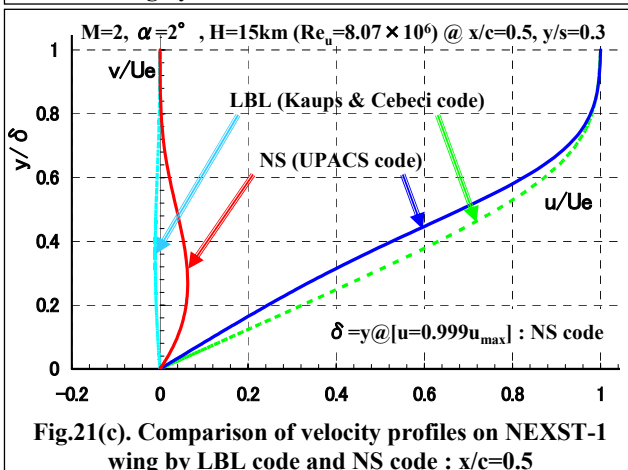
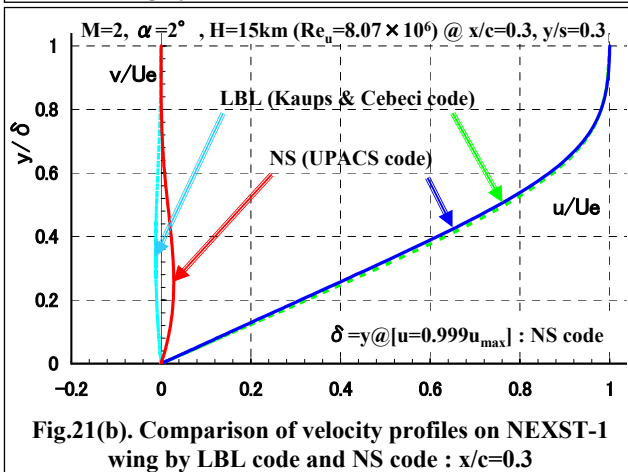
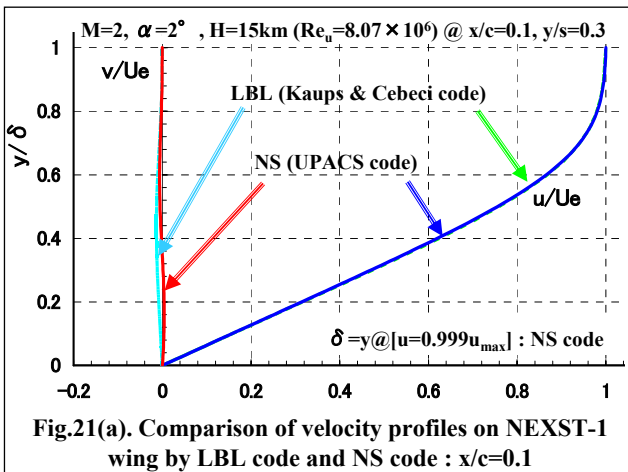
Figs. 21 show the velocity profiles at chordwise location $x/c=0.1, 0.3, 0.5$ on the 30% semi-spanwise station. First of all, a little difference is seen in the crossflow velocity profile at $x/c=0.1$. Further, the direction of the crossflow velocity is qualitatively and clearly opposite at $x/c=0.3$. Moreover, it is found out that there is also a remarkable difference even in the external streamwise velocity component (u) at $x/c=0.5$. In addition, an inflection point is

seen on the CFD-based profile at the vicinity of $x/c=0.5$.

Finally, the stability analysis was performed using those boundary layer profiles. The N factor distribution is shown in Fig. 22. It is seen in the figure that the estimated transition location corresponding to $N=12$ or more based on the profiles by the NS code is located rearward from that using the boundary layer

code [10]. Here, If $N=14$ is selected in the flight test condition with almost no freestream turbulence according to reference [16], the CFD-based transition prediction makes stand out the effect of our natural laminar flow wing design concept.

In addition, we set $x/c=0.6$ as a rearward limit in this study. The reason is as follows: it is difficult for the experimental airplane to maintain enough surface smoothness at $x/c>0.6$ because of the limitation of manufacturing and the control surfaces in the inboard wing. Therefore, the case of $N=14$ means that the N factor has not reached the value of 14 up to this limiting line.



As mentioned before, the validity of our natural laminar flow wing design concept was already qualitatively validated by the wind tunnel test [9] because of freestream turbulence in wind tunnel. Therefore, it is expected that the quantitative validation will be obtained only through the transition measurement in a flight test, which theoretically corresponds to no freestream turbulence condition. Moreover, by comparing the transition location pattern and transition analysis result on the wing, we consider that the effect of the analysis accuracy improvement of this approach is given a clear decision.

6 Concluding Remarks

In a transition analysis, an estimation accuracy of a boundary layer profile is important. We constructed the transition analysis system by the

application of the CFD code with high grid resolution. First of all, this system enables us to analyze the complicated transition phenomenon of the axisymmetrical bodies with non-zero angle of attack. The transition analysis of the sharp cone and the nose cone of the experimental airplane were performed. Consequently, it became clear that the transition location on the bottom line was moved rearward as the effect of angle of attack, and the transition locations on the top line and the side surface were moved forward significantly. They are dominated by the crossflow instability. In particular, the predicted transition location pattern of the sharp cone was also qualitatively equivalent to the wind tunnel test data.

The transition characteristics of the natural laminar flow wing of the scaled supersonic experimental airplane were analyzed by this procedure. Consequently, it was estimated that the natural laminar flow wing effect would be expanded more. However, remarkable difference of the N factor distribution between the CFD-based result and the result using the boundary layer code is only seen when the N factor is 12 or more.

References

- [1] D. Arnal. Boundary Layer Transition: Prediction Based on Linear Theory. *AGARD FDP/VKI Special Course on Progress in Transition Modeling*, AGARD Report 793, 1993
- [2] D. F. Fisher and N. S. Dougherty, Jr. In-Flight Transition Measurement on a 10° Cone at Mach Numbers from 0.5 to 2.0. *NASA TP-1971*, 1982
- [3] R. A. King. Three-dimensional Boundary-Layer Transition on a Cone at Mach 3.5. *Experiments in Fluids* 13, pp.305-314, 1992
- [4] M. Malik and P. Balakumar. Instability and Transition in Three-dimensional Supersonic Boundary Layers. *AIAA-92-5049*, 1992
- [5] K. Yoshida and Y. Makino. Aerodynamic Design of Unmanned and Scaled Supersonic Experimental Airplane in Japan. *Proceedings of ECCOMAS 2004*, 2004
- [6] M. R. Malik. COSAL – a Black-Box Compressible Stability Analysis Code for Transition Prediction in Three Dimensional Boundary Layer. *NASA CR-165925*
- [7] Yoshida, K., Ishida Y., Noguchi, M., Ogoshi, H., and Inagaki, K. Experimental and Numerical Analysis of Laminar Flow Control at Mach 1.4. *AIAA 99-3655*, 1999
- [8] K. Yoshida, T. Iwamiya, Y. Ueda and H. Ishikawa. Boundary Layer Transition Analysis of the Scaled Supersonic Experimental Airplane. *2nd International Workshop on Numerical Simulation Technology for Design of Next Generation Supersonic Civil Transport*, pp.85-90, January, 2000, Tokyo
- [9] H. Sugiura, K. Yoshida, N. Tokugawa, S. Takagi, and A. Nishizawa. Transition Measurement on the Natural Laminar Flow Wing at Mach 2. *J. Aircraft*, Vol.39, No.6, pp.996-1002, 2002
- [10] K. Kaups and T. Cebeci. Compressible Laminar Boundary Layers with Suction on Swept and Tapered Wings. *J. Aircraft* Vol.14, No.7, July, pp.661-667, 1977
- [11] Herring, H. J. and Mellor, G. L. Computer Program for Calculating Laminar and Turbulent Boundary Layer Development in Compressible Flow. *NASA CR-2068*
- [12] H. Sugiura, N. Tokugawa, K. Nishizawa, Y. Ueda, H. Ishikawa, K. Yoshida. Boundary-Layer Transition on Axisymmetric Bodies with Angles of Attack in Supersonic Flow. *Proceedings of 2003 Meeting of Japan Society of Fluid Mechanics*, 2003, pp.352-353 (in Japanese)
- [13] T. Cebeci and J. Cousteix. *Modeling and Computation of Boundary-layer Flows*. p.405, Springer, 1999
- [14] T. Atobe. Transition Analysis of Boundary Layers in Supersonic Flow Using a Complex Ray Theory. *NAL TR-1463*, 2003 (in Japanese)
- [15] R. Takaki, K. Yamamoto, T. Yamane, S. Enomoto, and J. Mukai. The Development of the UPACS CFD Environment. In A. Veidenbaum, K. Joe, H. Amano, and H. Aiso, editors, *High Performance Computing, 5th International Symposium, ISHPC 2003*, Tokyo-Odaiba, Japan, October 2003. Proceedings, volume 2858 of Lecture Notes in Computer Science, pages 307-319, Springer, 2003
- [16] R. D. Joslin. Aircraft Laminar Flow Control. *Annual Review of Fluid Mechanics*, Vol.30, pp.1-20, 1998